

Brown, K.L., Hart, W.K., and Stuck, R.J., 2018, Temporal and geochemical signatures in granitoids of northwestern Nevada: Evidence for the continuity of the Mesozoic magmatic arc through the western Great Basin: *Lithosphere*, <https://doi.org/10.1130/L694.1>.

GSA DATA REPOSITORY ITEM 2018123

ANALYTICAL METHODS

Petrography

A comprehensive suite of samples was collected from each of the main granitoid intrusions in the SRR-BRH. These intrusions include the Granite Peak stock, Santa Rosa pluton, Sawtooth stock, Andorno stock, Flynn stock, and the Bloody Run stock (Fig. 2). All samples used in this study were cut using standard diamond saws at Miami University and shipped to Spectrum Petrographics for thin/polished section preparation and mounting. Using a standard petrographic microscope and a Swift point counting stage attached to a 19 channel Prior (model G) point counting system, approximately 1500 point counts were collected on each section to establish modal mineralogy (Table 1).

U-Pb Zircon Geochronology

Heavy mineral separates (i.e. zircon, monazite, apatite, sphene) were isolated from approximately 2-3 kilograms of crushed rock using a Xtruder MSI mining gold shake table. Final zircon separates were achieved using a Frantz magnetic separator and heavy liquids techniques established at the Laserchron Center in the Department of Geological Sciences at the University of Arizona (www.laserchron.org). Approximately 50 to 100 grains from each of the final zircon separates were selected and incorporated into a 1" epoxy mount along with fragments of seven zircon standards (Mud Tank, 91500, Temora, R33, FC52, Plesovice, and Sri Lanka). Each mount was imaged with a SEM using backscatter and cathodoluminescence (CL) modes. Color CL images were acquired using a Hitachi 3400N SEM (equipped with Gatan Chroma CL2 color/UV and Oxford EDS/EBSD detectors). These images were used to aid in the placement of laser pits and in the interpretation of the origin of each grain and its internal textures.

U-Pb zircon geochronology was conducted by laser ablation multi-collector inductively coupled plasma mass spectrometry (LA-MC-ICP-MS) at the University of Arizona using methods described by Gehrels et al. (2008). Using a spot diameter of 30 μm , individual zircon grains were ablated to a depth of $\sim 15 \mu\text{m}$ with a Photon Machines Analyte G2 Excimer laser (193nm). Following the method of Gehrels et al. (2008), each analysis consisted of one fifteen-second integration on peaks with the laser off (for backgrounds), fifteen one-second integrations (on peaks) while the laser is firing, and a thirty second delay to purge the sample for the next analysis.

Each session started and ended by collecting five to ten Sri Lankan zircon analyses to ensure the accuracy of all fractionation and interference corrections. Corrections for the interference of mercury were made by monitoring ^{202}Hg and using the natural ratio of $^{202}\text{Hg}/^{204}\text{Hg}$ to subtract the Hg contribution from mass 204 (e.g. Cecil et al., 2011). For each of the SRR-BRH samples, approximately 20 to 50 unknown zircon grains were analyzed using the same acquisition parameters used to analyze zircon standards. Fractionation between U and Pb was accounted for by bracketing every three to five unknown zircon measurements with the analysis of a Sri Lankan zircon standard (accepted ID-TIMS age = $563.5 \pm 3.2 \text{ Ma}$, 2σ , see Gehrels et al., 2008). During the analytical session, the weighted mean Sri Lankan zircon age was $563.8 \pm 1.3 \text{ Ma}$

(2σ), which is in excellent agreement with the accepted ID-TIMS age. Corrections for common Pb were made by measuring ^{204}Pb and assuming an initial Pb composition based on the Pb evolution model of Stacey and Kramers (1975) (see Gehrels et al., 2008; Gehrels and Pecha, 2014). Weighted mean ages were determined for each sample using standard routines in IsoPlot software (Ludwig, 2008). Uncertainties for reported ^{238}U - ^{206}Pb ages are ~ 1 – 2% (2σ) and include both a systematic error (typically ~ 1 – 2%) and an error associated with the scatter and precision of a set of measurements for a given sample ($\sim 1\%$, 2σ). For details of error analysis see Gehrels et al. (2008) and Gehrels and Pecha (2014). All U-Pb zircon analyses used in this study are presented in Table DR2.

Mineral Chemistry: Electron Microprobe Analyses

Plagioclase and hornblende mineral compositions were determined by wavelength-dispersive X-ray emission microanalysis using a CAMECA SX50 electron microprobe in the Department of Geological Sciences at Indiana University. All analyses were performed using an accelerating voltage of 15 kV. Major elements were analyzed using a 1 μm beam diameter, a sample current of 20 nA, and a peak counting time of 20 seconds. Mineral compositions are reported in weight-percent oxides (Tables DR3 and DR4).

Using hornblende and plagioclase mineral compositions, estimated solidus pressures and temperatures were determined for selected granodiorite samples from the Santa Rosa Pluton, Flynn stock, and Bloody Run stock. The other stocks were not analyzed because they lacked hornblende or did not contain a mineral assemblage appropriate for the Al-in-hornblende thermobarometer, as outlined by Anderson (1996) and Anderson et al. (2008). Estimated solidus crystallization pressures were calculated using the Al-in-hornblende barometer of Anderson and Smith (1995), which incorporates the effect of higher temperature on the total Al content of amphibole coexisting with plagioclase and quartz. Estimated solidus temperatures were calculated from the hornblende-plagioclase thermometer (reaction B) of Holland and Blundy (1994). Hornblende and plagioclase pairs used in these calculations are reported in Table 2.

Bulk Major and Trace Element Analyses

Using only high-purity alumina components, bulk samples were crushed at Miami University using standard rock preparation equipment and procedures. Major element concentrations were obtained on whole-rock fused glass discs at Franklin and Marshall College using a PANalytical 2404 X-ray fluorescence (XRF) vacuum spectrometer following the techniques of Mertzman (2000). All glass discs were analyzed for SiO_2 , Al_2O_3 , CaO , K_2O , P_2O_5 , TiO_2 , Fe_2O_3 , MnO , Na_2O and MgO . Major element calibrations used a suite of 55 international rock standards.

With the exception of scandium and nickel, all other trace element concentrations were obtained using a Varian quadrupole inductively coupled mass spectrometer (ICP-MS) at Miami University. Scandium and nickel were best analyzed by XRF, using the techniques described by Mertzman (2000). For ICP-MS analyses, roughly 400 mg of whole-rock sample powder was well-mixed with 800 mg of LiBO_2 flux. This mixture was then fused at 1000 $^\circ\text{C}$ for 30 minutes inside a muffle furnace. Molten sample-flux mixtures were fused into glass beads and dissolved in 60 mL of trace metal grade 5% HNO_3 . These solutions along with ten international rock standards and a blank were then analyzed by ICP-MS. International rock standards were used for calibrations and to determine accuracy and precision of each measurement. Uncertainties for Rb, Sr, Ba, Cs, V, Cr, Co, Cu, Zn, Ga, Y, and Ta are between 1-2% (2σ), and uncertainties for Zr, Nb, Yb, Hf, La, Ce, Pb, Th, and U are between 2-5% (2σ) of their reported values. A

representative set of major and trace element analyses is reported in Table 3. All major and trace element analyses are reported in Table DR5.

Sr and Nd Isotope Methods

Seventeen bulk rock granitoid samples were selected for Sr and Nd isotope analysis. Full details of dissolution and purification steps used are contained in Snyder (2005). Using aliquots of the same sample powders generated for major and trace element analyses, approximately 50 mg of each sample was dissolved in concentrated HF-HNO₃ followed by additional digestion steps using concentrated HNO₃ and HCl. Sr was separated and purified using Eichrom Sr cation exchange resin in 10 mL quartz glass columns. Purified Sr was then loaded on single Ta filaments with a tantalum oxide activator and analyzed by thermal ionization mass spectrometry (TIMS) on a Thermo-Finnigan Triton at Miami University. The measured ⁸⁷Sr/⁸⁶Sr ratio was corrected for mass fractionation using an ⁸⁶Sr/⁸⁸Sr ratio = 0.1194. The long-term external reproducibility (2σ) of Sr standard NBS987 at Miami University is ±0.000017 for ⁸⁷Sr/⁸⁸Sr with a running mean of 0.710239 (n = 174). Initial Sr isotope ratios were calculated using λ_{87Rb} = 1.42 × 10⁻¹¹ (yr⁻¹).

Using the bulk REE fraction eluted during Sr separations, Nd was separated and purified using Eichrom Ln Spec resin (AG1-X8) in 10 mL Bio Rad Polyp-Prep Chromatography Columns. Purified Nd was loaded on double Re filaments with a tantalum oxide activator and analyzed by TIMS on a Thermo-Finnigan Triton at Miami University. ¹⁴³Nd/¹⁴⁴Nd was corrected for fractionation using a ¹⁴⁶Nd/¹⁴⁴Nd ratio = 0.7219. The long-term external reproducibility (2σ) of the La Jolla Nd standard at Miami University is ±0.000008 for ¹⁴³Nd/¹⁴⁴Nd with a running mean of 0.511846 (n = 119). Initial Nd isotope ratios were calculated using λ_{147Sm} = 6.54 × 10⁻¹² (yr⁻¹). ¹⁴³Nd/¹⁴⁴Nd_i is reported as εNd relative to the chondritic uniform reservoir (CHUR) evolution model of Jacobsen and Wasserburg (1980). Elemental concentrations and isotope ratios of Sr and Nd are reported in Table 4.

Zircon Hf Isotope Analyses

Hf isotope analyses on individual zircon grains were collected at the Laserchron Center at the University of Arizona with a Nu HR ICPMS connected to a Photon Machines Analyte G2 excimer laser using methods outlined in Cecil et al. (2011) and Gehrels and Pecha (2014). *In-situ* Hf isotope data were acquired on unknown zircons using a 40 μm beam diameter (laser pulse frequency of 7 Hz) that was centered directly on top of the 30 μm pit previously excavated for U-Pb analysis. During the analytical session, CL images were examined to ensure that Hf ablation pits overlapped previously excavated U-Pb pits and avoided analyzing multiple age domains or inclusions. Each acquisition consisted of one forty-second integration on backgrounds (on peaks with no laser firing) followed by sixty one-second integrations with the laser firing (see Gehrels and Pecha, 2014). Analyses of unknown zircons were conducted with exactly the same acquisition parameters as zircon standards. Full details of the zircon Hf isotope method employed in this study are available in Cecil et al. (2011) and Gehrels and Pecha (2014). All zircon Hf isotope analyses are reported in Tables DR6 and DR7. The ¹⁷⁶Hf/¹⁷⁷Hf at time of crystallization is calculated from measurement of present-day ¹⁷⁶Hf/¹⁷⁷Hf and ¹⁷⁶Lu/¹⁷⁷Hf, and uses the decay constant of ¹⁷⁶Lu (λ = 1.865 × 10⁻¹¹; from Scherer et al., 2001 and Söderlund et al., 2004). Values of (¹⁷⁶Hf/¹⁷⁷Hf)_{CHUR}⁰ (= 0.282785) and (¹⁷⁶Lu/¹⁷⁷Hf)_{CHUR}⁰ (= 0.0336) are from Bouvier et al. (2008).

References (Analytical Methods)

- Anderson, J.L., 1996, Status of thermobarometry in granitic batholiths: Transactions of the Royal Society of Edinburgh: Third Hutton Symposium, The Origins of Granites and Related Rocks, v. 87, issue 1-2, p. 125-138.
- Anderson, J.L., Barth, A.P., Wooden, J.L., and Mazdab, F., 2008, Thermometers and Thermobarometers in Granitic Systems *in* Putirka, K.D., and Tepley III, F. J., (eds) Minerals, Inclusions, and Volcanic Processes: Reviews in Mineralogy and Geochemistry, v. 69, p.121-142.
- Anderson, J.L., and Smith, D.R., 1995, The effect of temperature and oxygen fugacity on Al-in-hornblende barometry: The American Mineralogist, v. 80, p. 549–559.
- Bouvier, A., Vervoort, J.D., and Patchett, P.J., 2008, The Lu-Hf and Sm-Nd isotopic composition of CHUR: Constraints from unequilibrated chondrites and implications for the bulk composition of terrestrial planets: Earth and Planetary Science Letters, v. 273, p. 48-57.
- Cecil, M., Gehrels, G., Ducea, M.N., and Patchett, J., 2011, U-Pb-Hf characterization of the central Coast Mountains batholith: Implications for petrogenesis and crustal architecture: Lithosphere, v. 3, p. 247-260.
- Gehrels, G.E., and Pecha, M., 2014, Detrital zircon U-Pb geochronology and Hf isotope geochemistry of Paleozoic and Triassic passive margin strata for western North America: Geosphere, v. 10, p. 49-65.
- Gehrels, G.E., Valencia, V., Ruiz, J., 2008, Enhanced precision, accuracy, efficiency, and spatial resolution of U-Pb ages by laser ablation-multicollector-inductively coupled plasma-mass spectrometry: Geochemistry, Geophysics, Geosystems, v. 9, Q03017.
- Holland, T., and Blundy, J., 1994, Non-ideal interactions in calcic amphiboles and their bearing on amphibole-plagioclase thermometry: Contributions to Mineralogy and Petrology, v. 116, p. 433–447.
- Jacobsen S.B., and Wasserburg, G.J., 1980, Sm-Nd isotopic evolution of chondrites: Earth and Planetary Science Letters, v. 50, p. 139-155.
- Mertzman, S. A., 2000, K-Ar results from the southern Oregon - northern California Cascade Range. Oregon Geology, v. 62, no. 4, pp. 99-122.
- Scherer, E., Münker, C., and Mezger, K., 2001, Calibration of the Lutetium-Hafnium Clock: Science, v. 293, issue 5530, p. 683–687.
- Söderlund, U., Patchett, P.J., Vervoort, J.D., and Isachsen, C.E., 2004, The ^{176}Lu decay constant determined by Lu-Hf and U - Pb isotope systematics of Precambrian mafic intrusions: Earth and Planetary Science Letters, v. 219, p. 311-324.
- Stacey, J.S., and Kramers, J.D., 1975, Approximation of terrestrial lead isotope evolution by a two-stage model: Earth and Planetary Science Letters, v. 26, p. 207-221.
- Snyder, D.C., 2005, Processes and time scales of differentiation in silicic magma chambers: chemical and isotopic investigations. PhD Dissertation, Miami University, 216p

Figure DR1a, DR1b, and DR1c. Representative SEM color cathodoluminescence (CL) images of zircons from the SRR-BRH granitoids showing U-Pb ages (yellow) and $\epsilon\text{Hf}(t)$ values (red). All reported ages are in millions of years. All $\epsilon\text{Hf}(t)$ values are age corrected using measured U-Pb zircon ages. Scale bars are 100 microns. Yellow circles represent 30 micron diameter U-Pb analyses. Red circles represent 40 micron $\epsilon\text{Hf}(t)$ analyses. Individual U-Pb zircon ages, isotope ratios, and uncertainties are present in Table DR2. Individual $\epsilon\text{Hf}(t)$ values, isotope ratios, and uncertainties are present in Tables DR6 and DR7.

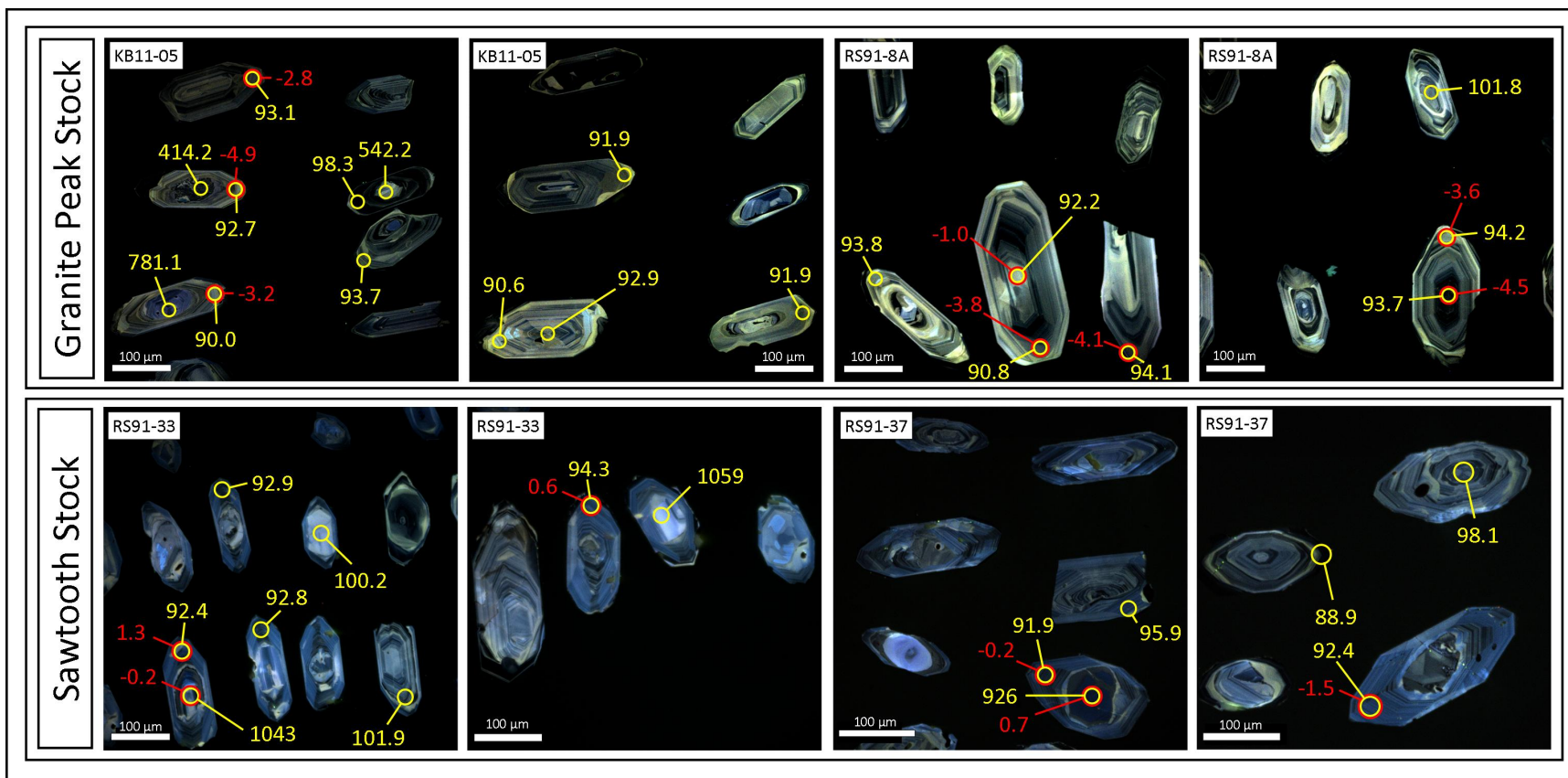


Figure DR1a

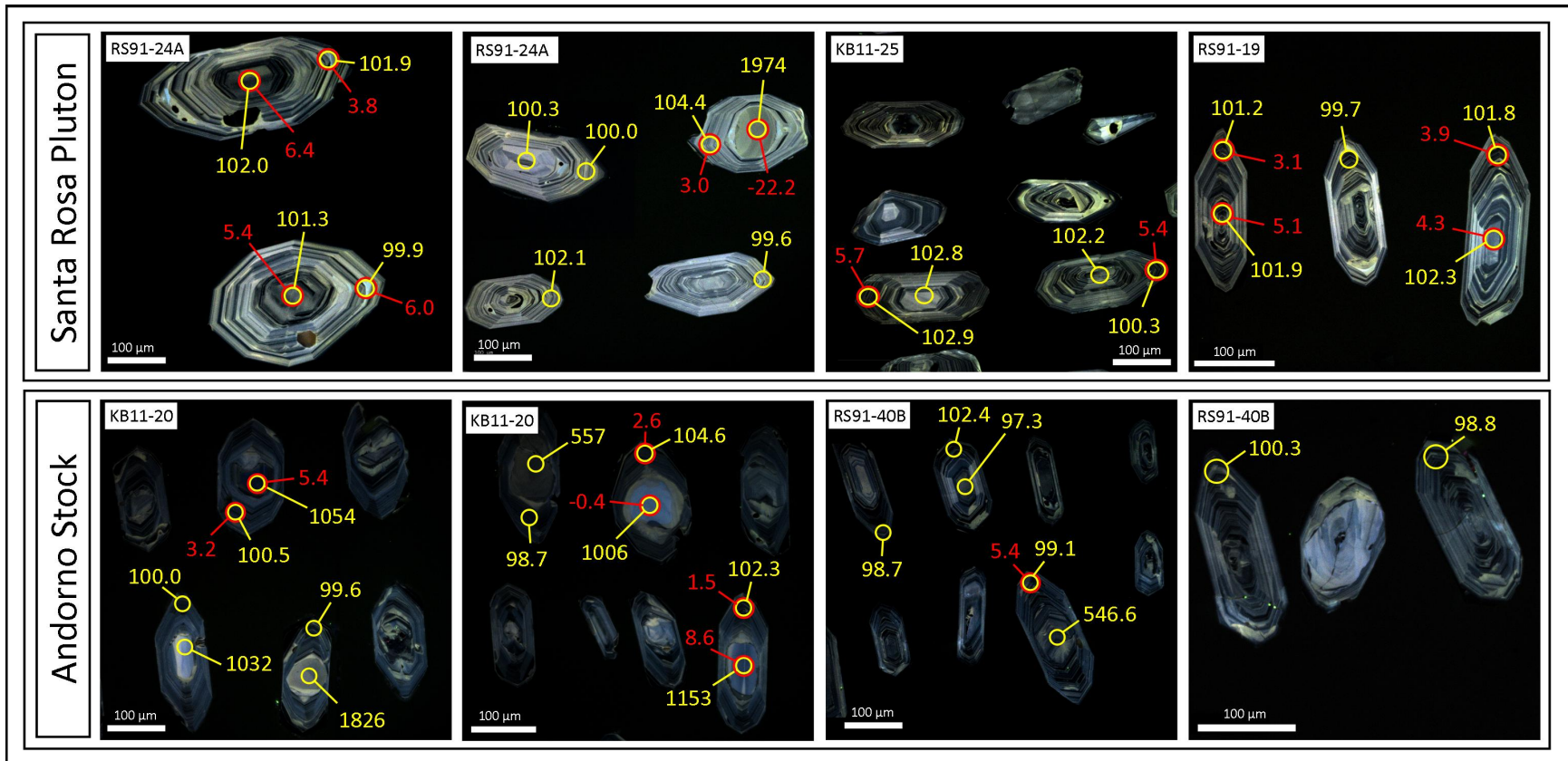


Figure DR1b

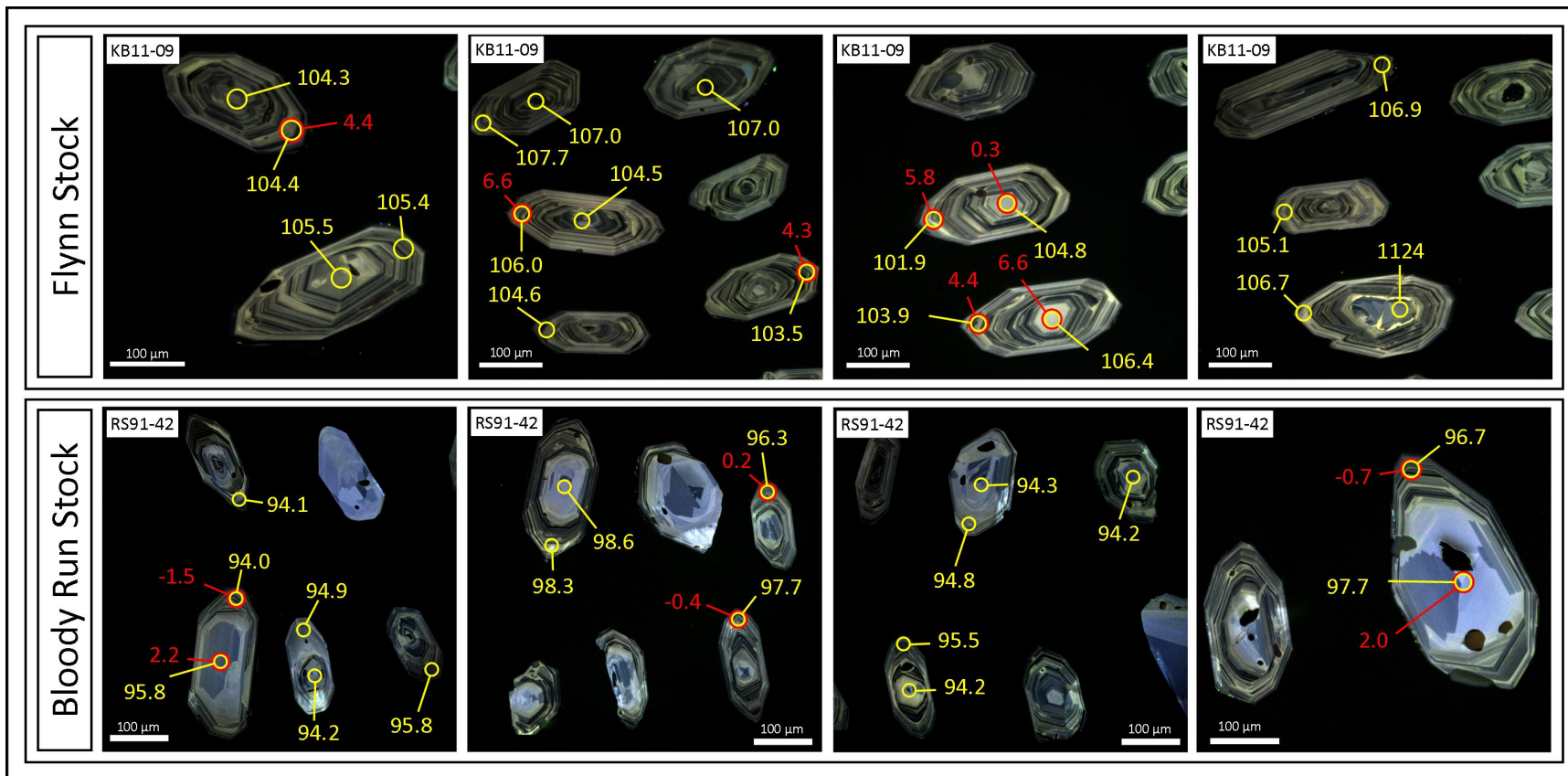


Figure DR1c

Figure DR2a, DR2b, and DR2c: Concordia diagrams (left) and weighted mean zircon U-Pb age plots (right) for selected SRR-BRH granitoid samples. Error ellipses (Concordia diagrams) and errors bars (weighted mean plots) are shown at the 2σ level. Quoted weighted mean ages for each sample include both the analytical uncertainty and a systematic uncertainty at the 2σ level (see Gehrels et al., 2008). All reported ages, including 2σ uncertainties, were generated using routines in Isoplot (Ludwig, 2008). Individual U-Pb analyses are reported in Table DR2.

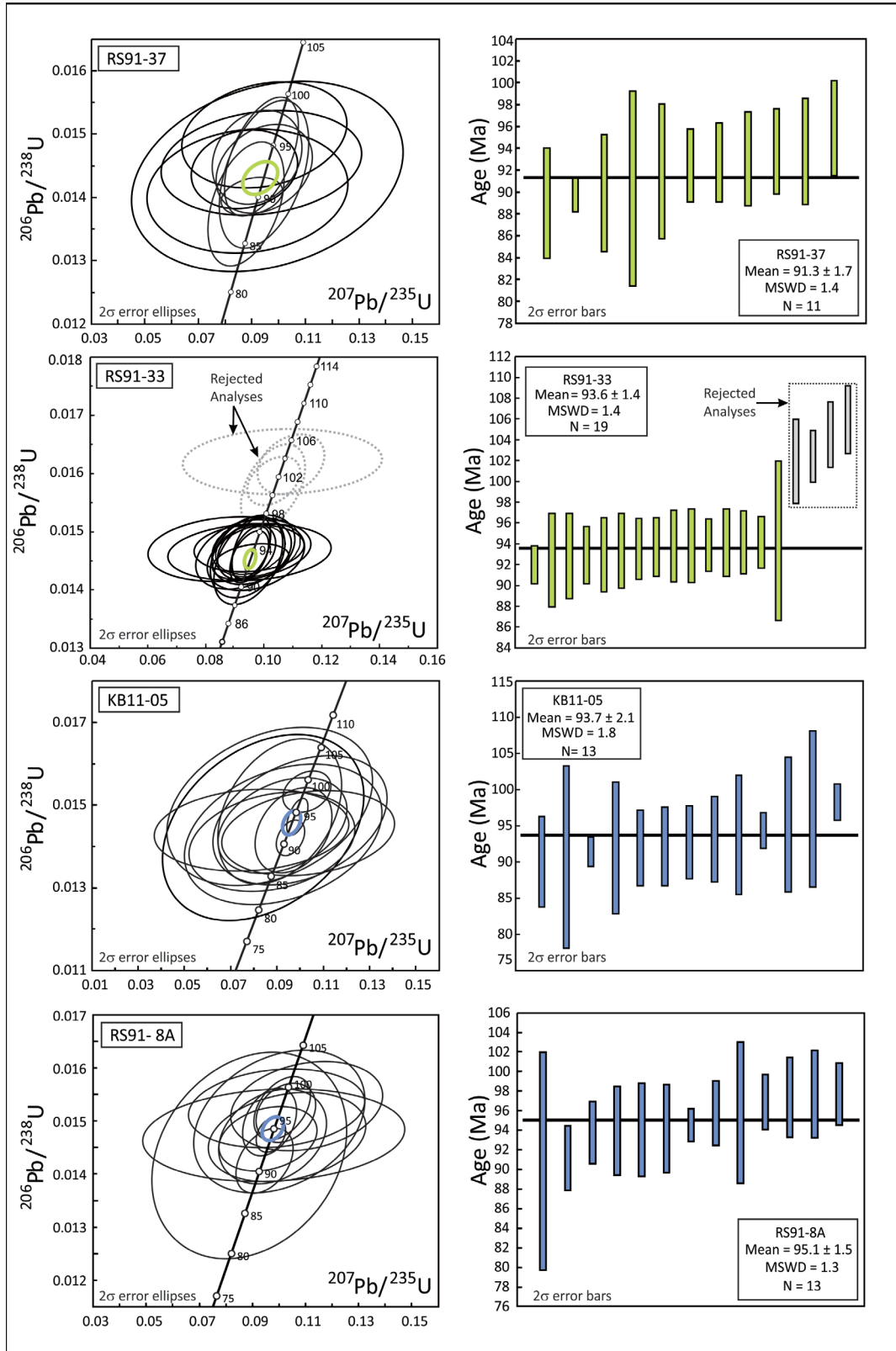


Figure DR2a

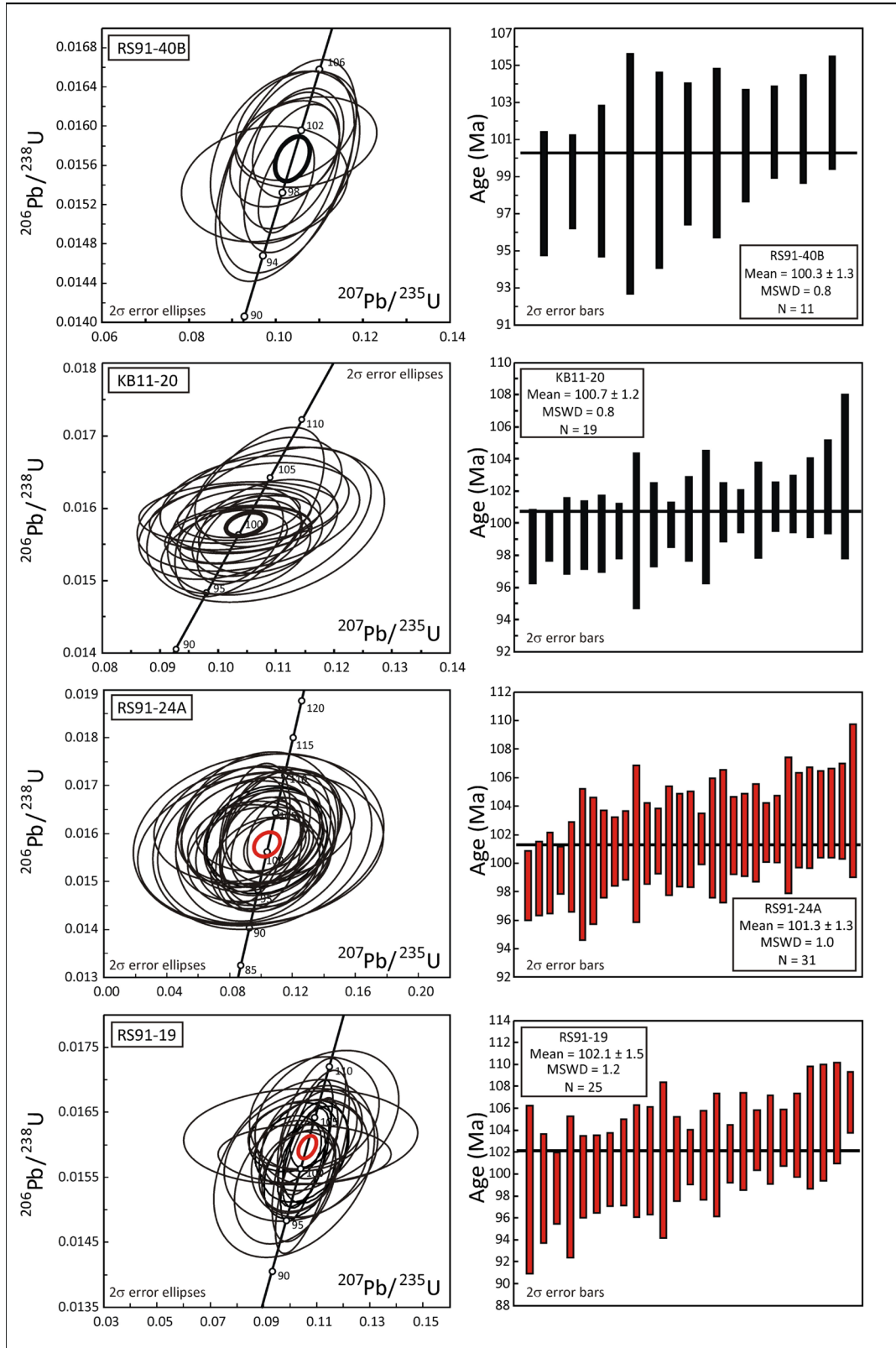


Figure DR2b

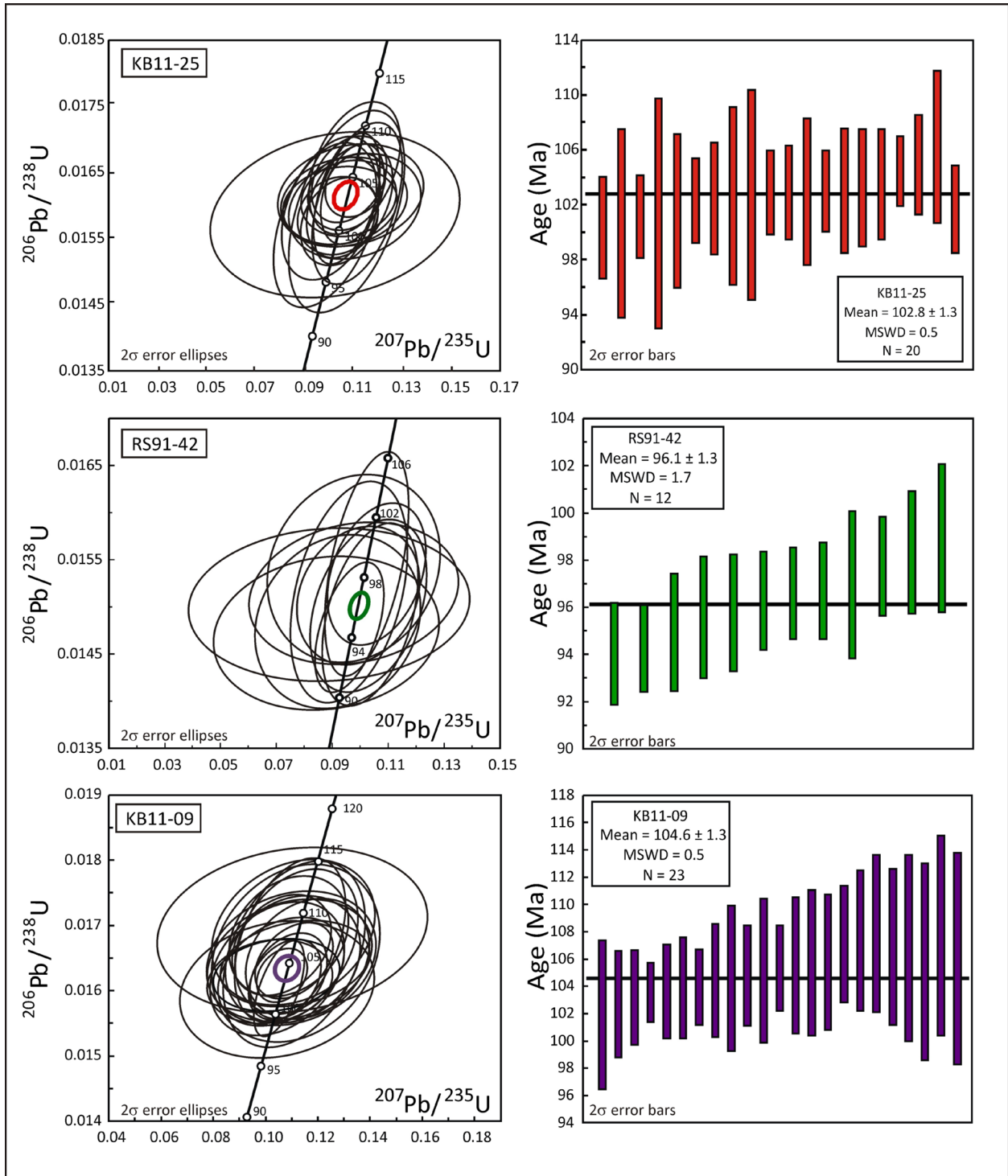


Figure DR2c

Figure DR3. A. Summary of plagioclase feldspar compositions for the SRR-BRH granitoids. Closed symbols represent plagioclase feldspar cores and open symbols represent plagioclase feldspar rims. Ab – albite; An – anorthite; Or – orthoclase. Individual analyses are reported in Table DR4. B. Results of Al-in-hornblende thermobarometry for the SRR-BRH granitoids. Estimated pressures based on Al-in-hornblende calibration of Anderson and Smith (1995) with temperature based on amphibole–plagioclase thermometry (reaction B) of Holland and Blundy (1994). Error bars represent 2 standard deviations of multiple mineral pairs (Santa Rosa pluton – n = 6, ± 0.5 GPa, $\pm 14^\circ\text{C}$; Bloody Run stock – n = 3, ± 0.4 GPa, $\pm 26^\circ\text{C}$; Flynn stock – n = 6, ± 0.4 GPa, $\pm 16^\circ\text{C}$). Granite and Tonalite solidii from Anderson et al. (2008). Individual hornblende analyses are reported in Table DR3. Hornblende-Plagioclase pairs are reported in Table 2.

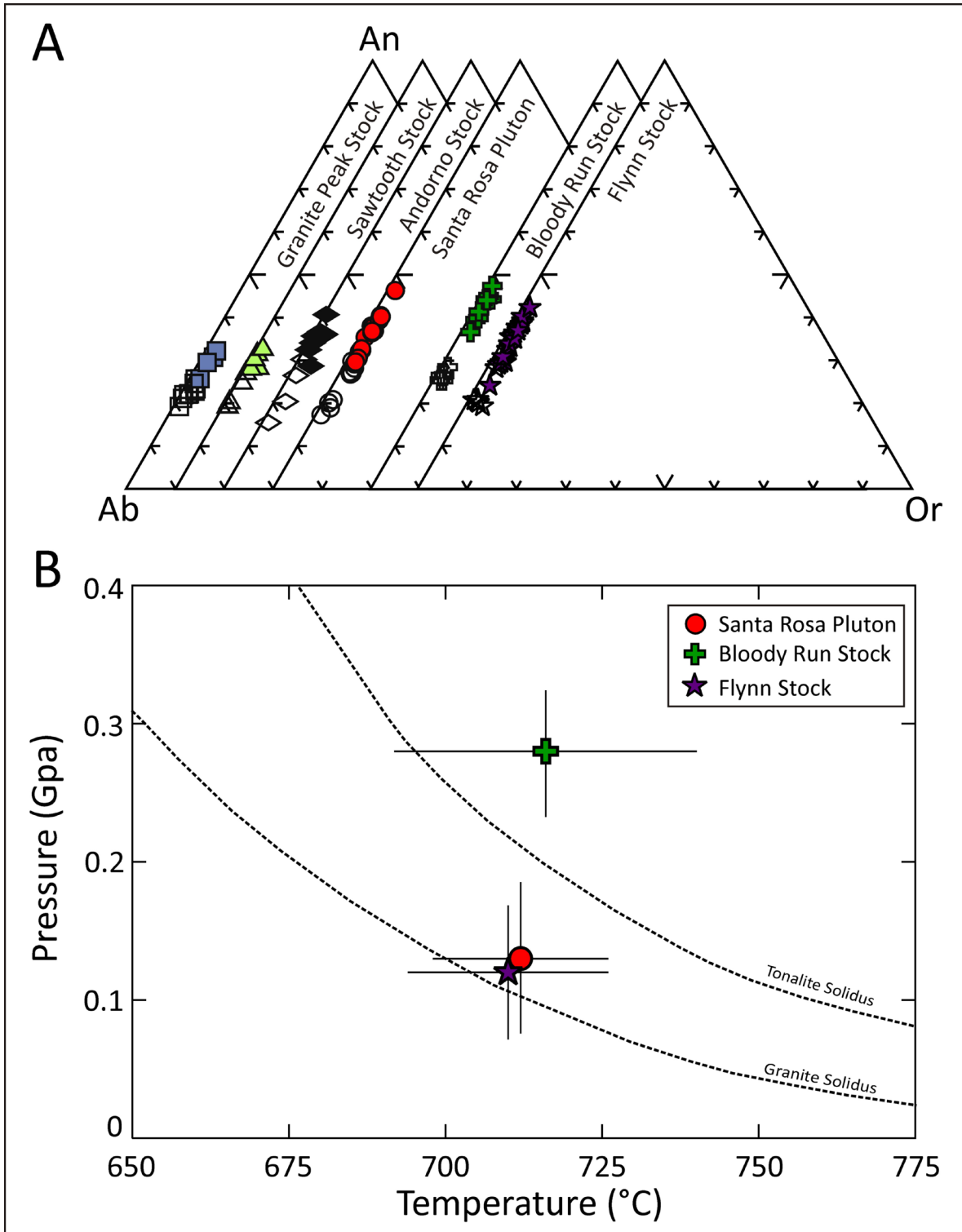


Figure DR3

Figure DR4: A. $\epsilon\text{Hf}_{(t = \text{U-Pb zircon age})}$ values from interpreted autocrystic core-rim zircon pairs for the SRR-BRH granitoids. Error bars (upper left) show average 2σ uncertainties (± 3.2 Ma; ± 3.0 ϵHf units). All $\epsilon\text{Hf}_{(t)}$ values were age corrected using measured U-Pb zircon ages (i.e. timing of zircon crystallization). Dotted arrow indicates core to rim direction. Insert (lower right) contains color CL image of interpreted autocrystic core-rim zircon pair (KB11-09), showing $\epsilon\text{Hf}_{(t)}$ values and corresponding U-Pb ages (Ma). B. $\epsilon\text{Hf}_{(t = \text{U-Pb zircon age})}$ values from interpreted xenocrystic core - autocrystic rim pairs for the Santa Rosa granitoids. All $\epsilon\text{Hf}_{(t)}$ values were age corrected using measured U-Pb zircon ages (i.e. timing of zircon crystallization). Dotted arrow indicates core to rim direction. U-Pb age error bars are within the size of each symbol. $\epsilon\text{Hf}_{(t)}$ error bars are shown at 2σ level. Insert (upper right) contains color CL image of interpreted xenocrystic core and autocrystic rim pair (RS91-24A), showing corresponding $\epsilon\text{Hf}_{(t)}$ values and U-Pb ages (Ma). $\epsilon\text{Hf}_{(t)}$ values, U-Pb ages, and 2σ uncertainties are reported in Tables DR6 and DR7.

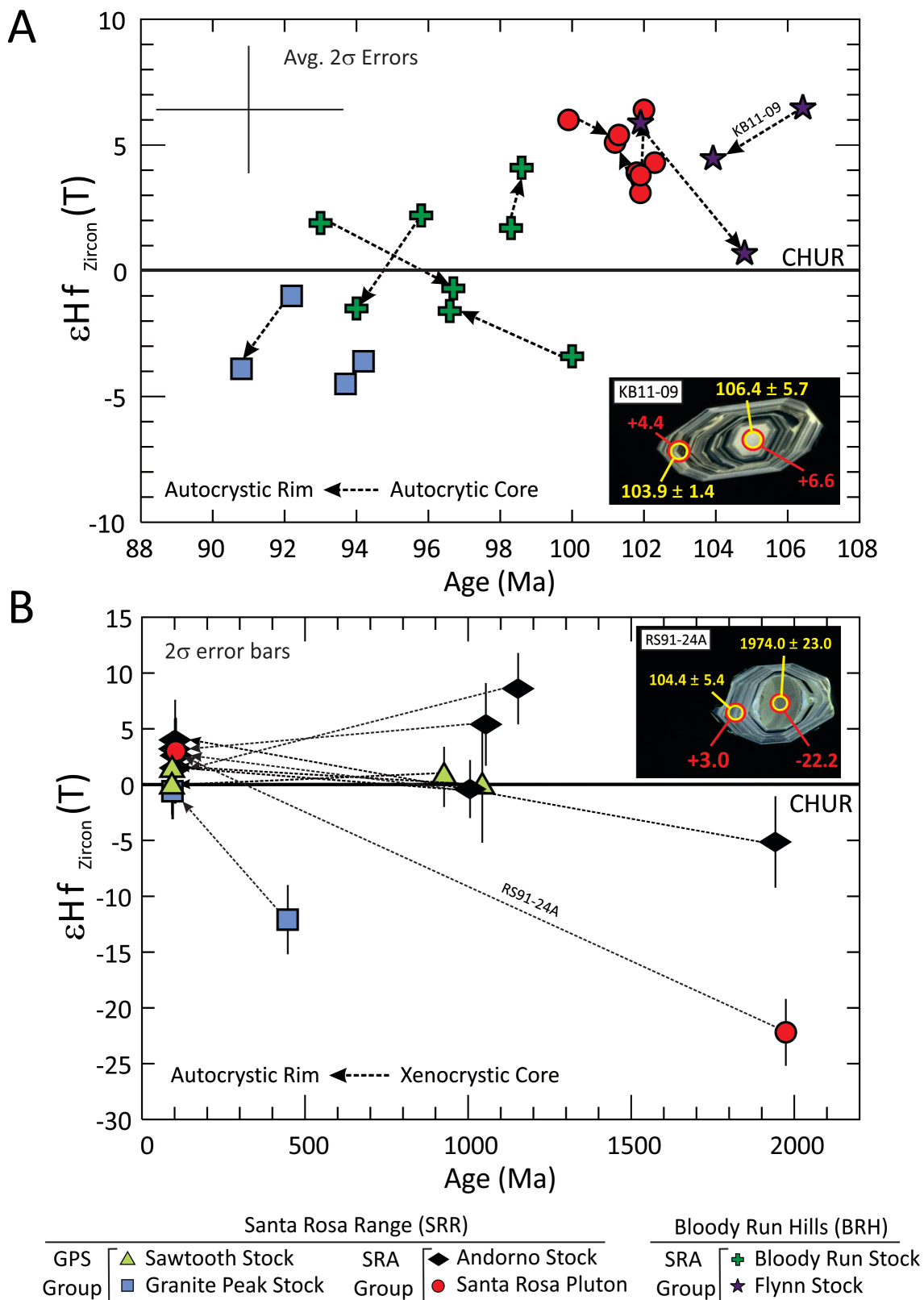


Figure DR4

Figure DR5: (Figure 10 – Full image). A. Concordia diagram of all xenocrystic zircon cores (n = 64) for the SRR-BRH granitoids. Error ellipses are shown at the 2σ level. B. Histogram (red boxes) and probability density plot (thick black line) of U-Pb ages from all xenocrystic zircon cores for the SRR-BRH granitoids. Shaded vertical bars represent the age range of basement provinces in North America (after Gehrels and Pecha, 2014). C. (Top) Probability density plot of all xenocrystic zircons from the SRR-BRH granitoids (thick red line) compared to detrital zircon populations from Triassic sedimentary rocks within Nevada and Utah (Chinle and Osobb Formations; Gehrels and Pecha, 2014). Note - not all xenocrystic zircon grains were analyzed for Hf isotope analyses. (Bottom) $\epsilon\text{Hf}_{(t = \text{U-Pb zircon age})}$ values for xenocrystic zircon cores from the SRR granitoids compared to detrital zircons from Triassic sedimentary rocks within Nevada and Utah (Chinle and Osobb Formations; Gehrels and Pecha, 2014). Error bars are shown at the 2σ level. All $\epsilon\text{Hf}_{(t)}$ values are age corrected to the measured U-Pb zircon ages.

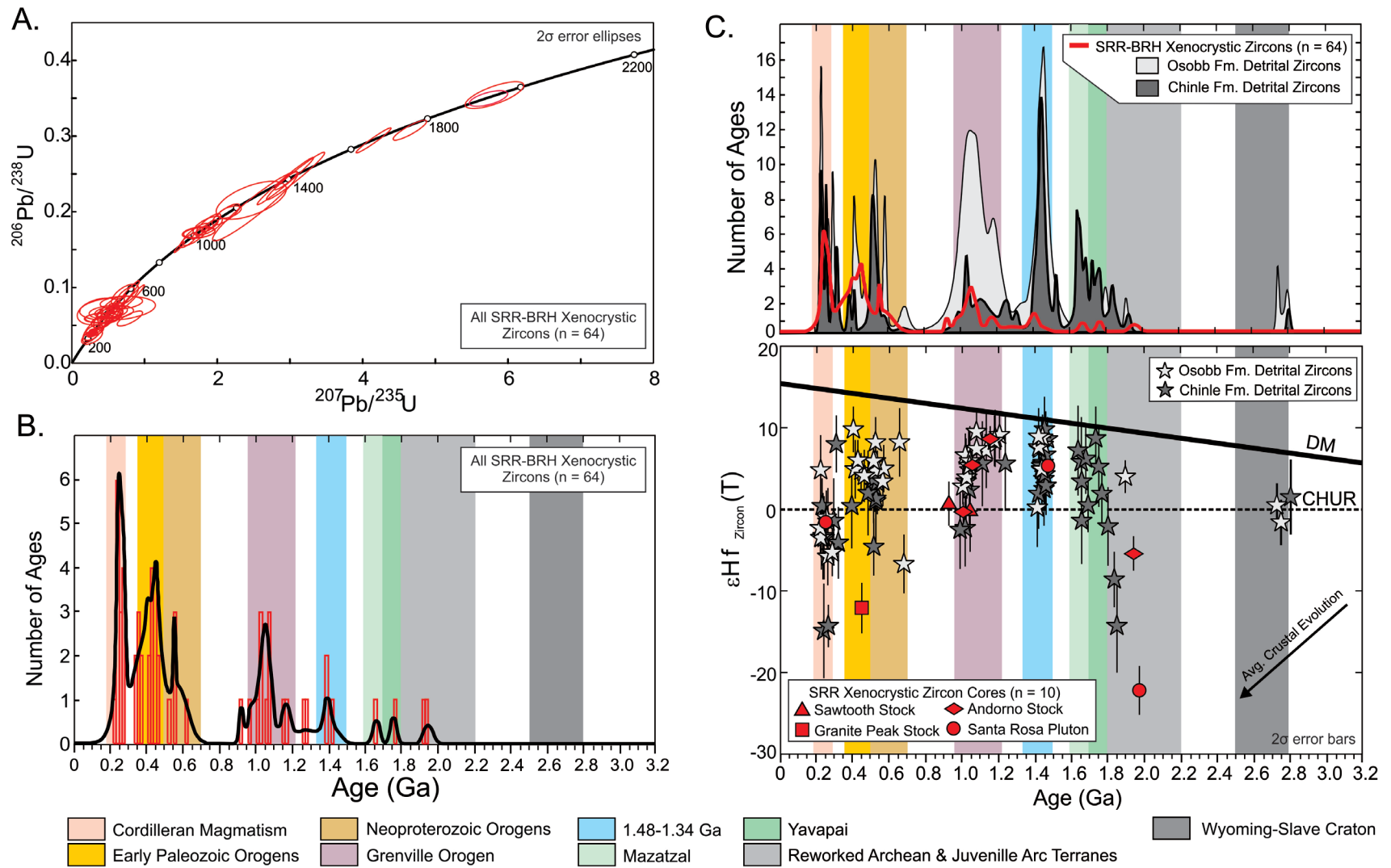


Figure DR5